



# Arecibo measurements of D-region electron densities during sunset and sunrise: implications for atmospheric composition

Carsten Baumann<sup>1</sup>, Antti Kero<sup>2</sup>, Shikha Raizada<sup>3</sup>, Markus Rapp<sup>4,5</sup>, Michael P. Sulzer<sup>3</sup>, Pekka T. Verronen<sup>2,6</sup>, and Juha Vierinen<sup>7</sup>

<sup>1</sup>Deutsches Zentrum für Luft- und Raumfahrt, Institut für Solar Terrestrische Physik, Neustrelitz, Germany

<sup>2</sup>Sodankylä Geophysical Observatory, Oulu University, Sodankylä, Finland

<sup>3</sup>National Astronomy and Ionosphere Center, Arecibo Observatory, Arecibo, Puerto Rico

<sup>4</sup>Deutsches Zentrum für Luft- und Raumfahrt, Institut für Physik der Atmosphäre, Wessling, Germany

<sup>5</sup>Meteorologisches Institut, Ludwig-Maximilians Universität, Munich, Germany

<sup>6</sup>Space and Earth Observation Centre, Finnish Meteorological Institute, Helsinki, Finland

<sup>7</sup>Department of Physics and Technology, UiT The Arctic University of Norway, Tromsø, Norway

**Correspondence:** Carsten Baumann (carsten.baumann@dlr.de)

Received: 25 March 2022 – Discussion started: 31 March 2022

Revised: 27 June 2022 – Accepted: 4 July 2022 – Published: 2 August 2022

**Abstract.** Earth's lower ionosphere is the region where terrestrial weather and space weather come together. Here, between 60 and 100 km altitude, solar radiation governs the diurnal cycle of the ionized species. This altitude range is also the place where nanometre-sized dust particles, recondensed from ablated meteoric material, exist and interact with free electrons and ions of the ionosphere. This study reports electron density measurements from the Arecibo incoherent-scatter radar being performed during sunset and sunrise conditions. An asymmetry of the electron density is observed, with higher electron density during sunset than during sunrise. This asymmetry extends from solar zenith angles (SZAs) of 80 to 100°. This D-region asymmetry can be observed between 95 and 75 km altitude. The electron density observations are compared to the one-dimensional Sodankylä Ion and Neutral Chemistry (SIC) model and a variant of the Whole Atmosphere Community Climate Model incorporating a subset SIC's ion chemistry (WACCM-D). Both models also show a D-region sunrise–sunset asymmetry. However, WACCM-D compares slightly better to the observations than SIC, especially during sunset, when the electron density gradually fades away. An investigation of the electron density continuity equation reveals a higher electron–ion recombination rate than the fading ionization rate during sunset. The recombination reactions are not fast enough to closely match the fading ionization rate during sunset, re-

sulting in excess electron density. At lower altitudes electron attachment to neutrals and their detachment from negative ions play a significant role in the asymmetry as well. A comparison of a specific SIC version incorporating meteoric smoke particles (MSPs) to the observations revealed no sudden changes in electron density as predicted by the model. However, the expected electron density jump (drop) during sunrise (sunset) occurs at 100° SZA when the radar signal is close to the noise floor, making a clear falsification of MSPs' influence on the D region impossible.

## 1 Introduction

The D region is not only the lowest part of the ionosphere but also the faintest, with its low abundance of free electrons. Only few measurement techniques allow investigations of this peculiar ionospheric region, i.e. rocket-borne in situ measurements (e.g. Friedrich and Rapp, 2009, and references therein), interpretation of very low-frequency (VLF) radio wave reflections (e.g. Han and Cummer, 2010; Maurya et al., 2012), partial reflection of medium-frequency (MF) radio waves (e.g. Reid, 2015, and references therein), and its sensing by means of incoherent scatter from free electrons. The latter technique was performed with the Arecibo incoherent-scatter radar (ISR) in Puerto Rico from 1963 until

1 December 2020 with its large 305 m dish and 2.5 MW radio wave transmitter (e.g. Isham et al., 2000, and references therein). This work aims to report specific sunset and sunrise D-region measurements performed with this one-of-a-kind radar during the end of August 2016.

The transmitted electromagnetic radar wave of the ISR is scattered from the ionospheric plasma. The detected backscattered signal can be described with Thomson scatter theory (Tanenbaum, 1968; Evans, 1969), which is adjusted for the collisional D-region plasma (Mathews, 1978). ISR measurements of the D region have a long history and reach back to the beginning of the operation of high-power large-aperture radars like in Arecibo or elsewhere (e.g. Mathews et al., 1982; Kudeki et al., 2006; Raizada et al., 2008; Kero et al., 2008).

The first ISR investigations of the D-region ionosphere, especially during sunset and sunrise, were performed by Trost (1979). However, they did not investigate the differences between sunset and sunrise in detail. Other methods including MF radar (e.g. Coyne and Belrose, 1972; Li and Chen, 2014) and radio propagation methods (e.g. Laštovička, 1977) have also been used to investigate the D region during these times and discovered an asymmetry in the observed electron densities.

These observations led to further studies that investigated the interaction of the D region with the background atmosphere. While Mathews et al. (1982) found gravity wave activity within the electron density measurements, Forbes (1981) investigated the influence of tides on the D-region ion chemistry based on the temperature dependence of reaction coefficients. The role of positive-ion chemistry and its dependence on solar zenith angle and temperature plays a role during times of low ionization (Forbes, 1982). The importance of the neutral atmosphere has also been identified from diurnal variations in the temperature to the neutral-density quotient inferred from the spectral width of ISR signals (Ganguly, 1985).

Satellite observations of nitric oxide, i.e. the main ionized species in the D region (Nicolet and Aikin, 1960), show a distinct asymmetry in the NO concentration during sunset and sunrise (Siskind et al., 1998) as well. Friedrich et al. (1998) investigated these satellite results with respect to the D-region electron density and concluded that diurnal NO variations should be investigated within ionospheric models. Also atomic oxygen plays a prominent role in the lowermost D region and underlies a diurnal cycle to be taken into account for ionospheric modelling (Siskind et al., 2015).

Finally, ISR spectra from the lower ionosphere depend not only on the number of free electrons but also on the composition of the ions and abundance of charged aerosols. One peculiarity of the D region is the possibility that negative ions can exist. Another one is the co-existence of the plasma with so-called meteoric smoke particles, which recondense from ablated meteoric material (Hunten et al., 1980). Cho et al. (1998) postulated a modification of ISR spectra due

to the presence of heavy negative-charge carriers. A later measurement campaign reported in Strelnikova et al. (2007) successfully measured D-region ISR spectra that could be explained with the presence of negatively charged meteoric dust particles with a mean radius of around 1 nm. The existence of charged meteoric smoke particle (MSP) dust has also been proven by means of rocket-borne dust detections (e.g. Rapp et al., 2012; Robertson et al., 2013). This type of charged dust measurements, including electron and positive-ion measurements revealed that negatively charged dust influences the charge balance within the nighttime D region (Friedrich et al., 2012). Modelling of the D region later confirmed this finding of Friedrich et al. (2012) (Baumann et al., 2013; Plane et al., 2014; Asmus et al., 2015). A comprehensive review on the lower ionosphere that covers its complexity in full breadth has been published by Friedrich and Rapp (2009).

The scope of this work is to interpret the sunset and sunrise electron density observations with the help of modern ionospheric models. The measurements are compared to the Sodankylä Ion and neutral Chemistry (SIC) model (Turunen et al., 1996), a one-dimensional model, and a variant of the global circulation model (GCM) Whole Atmosphere Community Climate Model including a subset of the SIC ion chemistry scheme (WACCM-D; Verronen et al., 2016). By doing so, it is possible to distinguish between dynamical drivers and the pure ionospheric processes on the observed D-region asymmetry.

A further aspect of this study is to identify the expected impact of MSPs on the electron density during sunset and sunrise based on earlier model results (Baumann et al., 2015). Electrons effectively attach to MSPs when the D region is in darkness, resulting in a sudden decrease in free electrons after sunset. The opposite occurs during sunrise when the sun starts to shine on D-region altitudes; large numbers of electrons are then photodetached from negatively charged MSPs. The electron density measurements are expected to pin down if MSPs are actually an effective sink of electrons during unilluminated times.

The study is structured as follows. The Arecibo ISR measurements of the electron density are presented in Sect. 2. Section 3 compares these measurements with results from the SIC and WACCM-D model. The observed D-region asymmetry is analysed in the “D-region asymmetry” section. The results of the analysis are discussed in Sect. 4, and the conclusions are summarized in Sect. 5.

## 2 Arecibo D-region measurements

The Arecibo radar consisted of the 305 m spherical antenna and a 430 MHz transmitter fed by a klystron RF amplifier. Its peak transmit power of up to 2.5 MW together with its high antenna gain of 61.1 dB makes the Arecibo facility the most sensitive ISR in the world. The radar experiment was

specially tailored for measuring the D-region electron densities. As a consequence a good measure of the background noise is crucial as it has to be subtracted from the backscattered power. Finally, the power profiles were calibrated using a plasma line measurement.

The details of this D-region radar experiment are as follows: the power profiles are obtained using an 88 baud code with a  $176\ \mu\text{s}$  RF pulse length. It is used with a  $400\ \mu\text{s}$  gate delay and 500 range gates with a  $2\ \mu\text{s}$  gate width. That results in an altitude range from 60 to 600 km. The “noise” measurement uses a 2 baud ( $\pm$ ) code with a  $0.2\ \mu\text{s}$  RF pulse length. By using the shortest input pulse length, the transmitter had no time to ramp up the power. As a consequence, the transmitted power was near zero, enabling a dedicated noise measurement. The 88 baud power profile and noise measurement used a 10 ms interpulse period, running in a sequence of 5 s each. The plasma line measurement was done using a coded long pulse sequence (Sulzer, 1986) with a  $440\ \mu\text{s}$  RF pulse length. The upper plasma line frequency was recorded in the frequency range of 5.5 to 9.5 MHz with 4.8 kHz resolution. This plasma line measurement was done for approximately 5 min before (after – for sunrise) the main experiment sequence described above. The plasma line measurements were possible down to approximately 120 km.

The measured plasma line frequency can be related to the plasma frequency (and consequently the local electron density) using the formalism of Yngvesson and Perkins (1968). The measured power profile is directly proportional to the electron density after subtraction of the noise and correction of the resulting signal for range and near-field antenna gain effects (Breakall and Mathews, 1982). This quantity is then calibrated with the measured electron density, resulting in a calibrated electron density profile from 60 to 600 km. We assume a constant calibration during the 4 h experiment period. Figure 1 shows the result of this procedure after coherent integration of four sequences, resulting in 40 s time resolution and 300 m altitude resolution. The figure contains four sunset (28–31 August) and two sunrise measurements (29 August and 1 September). Due to technical difficulties, the sunrise measurements on 29 and 30 September were unsuccessful. The time axis of the measured electron densities is transferred to solar zenith angle for a better comparison. The expected behaviour of declining electron density with SZA is visible in all altitudes. However, there are differences between the sunset and sunrise data. Between 95 and 120 km sporadic E layers are present during nearly the whole measurement period (e.g. Hysell et al., 2009). These layers are related to metal ion layers and atmospheric wind shears in these altitudes (e.g. Whitehead, 1961; Raizada et al., 2011). Unfortunately, radio clutter occurs at lower altitudes with different severity as well. This originates from radar beam side lobe reflections of aeroplanes and ships at these range gates.

Geomagnetic activity during the measurement period was low to moderate, with Kp index ranging from 0 to 4. The DST index reached a minimal value of  $-57\ \text{nt}$  on 1 September

2016 10:00 UTC at the very end of the measurement campaign. This enhanced geomagnetic activity. The activity of the sun was moderate, with radio flux F10.7 ranging between 80 and 100 sfu. The strongest solar flare was of type C2.2 and occurred on 31 August 20:19 UTC (GOES), but no immediate impact on the D region is visible in the data.

To directly compare sunset and sunrise data, Fig. 2 shows measured electron densities at different altitudes from 95 down to 70 km as a function of SZA. The shown data represent the mean of the two sunrise and four sunset measurements. For the case of the sunset dataset a 25 % trimmed mean (e.g. Wilcox, 2011) is shown; doing that removes one strong outlier from the four observations due to either sporadic E layers, low-altitude interference from ships and planes, or data gaps during periods when the transmitter was off. Furthermore, the shown lines represent the 20-point running mean, and the shaded regions indicate the standard deviation of this running mean. At low SZA the electron densities are remarkably similar for sunset and sunrise. However, as the sun reaches around  $80^\circ$  SZA, sunset and sunrise measurements start to deviate.

At 95 km altitude the sunset electron density starts being higher than during sunrise at around  $75^\circ$  already. This asymmetry remains in place for all SZAs higher than that. However, this altitude region is likely influenced by the presence of sporadic E layers that are very frequent in the evenings. The D-region asymmetry for 90 km starts at  $85^\circ$  SZA and also remains present for all higher SZAs as well. For 85 km altitude, the asymmetry starts at  $85^\circ$  SZA as well. But the electron density values match later at around  $100^\circ$  SZA again. At 80 km altitude the D-region asymmetry is not so pronounced as in the altitude regions above but also starts at  $85^\circ$  SZA and ends at  $100^\circ$ . The situation is more clear at 75 km altitude again. Here, the asymmetry already starts at  $80^\circ$  and extends until  $100^\circ$  SZA. At 70 km a clear asymmetry cannot be observed anymore because the signal-to-noise ratio of the measurement is too low here.

The increasing standard deviation of the measurements indicates that the measured electron densities are close to or at the noise floor of the Arecibo radar. The SZA at which the standard deviation sharply increases varies with not only altitude but also sunset or sunrise. The noise floor is reached at larger SZAs during sunset than during sunrise. This behaviour indicates a sunset–sunrise asymmetry of the ionosphere at altitudes from 90 to 75 km as well.

### 3 Comparison with ionospheric models

This section compares the electron density measurements to the Sodankylä Ion- and neutral-Chemistry (SIC) model (Turunen et al., 1996) and WACCM-D (Verronen et al., 2016).

We apply the SIC model in its original version and the version including meteoric smoke particles (Baumann et al., 2015). The SIC model is a one-dimensional ionospheric

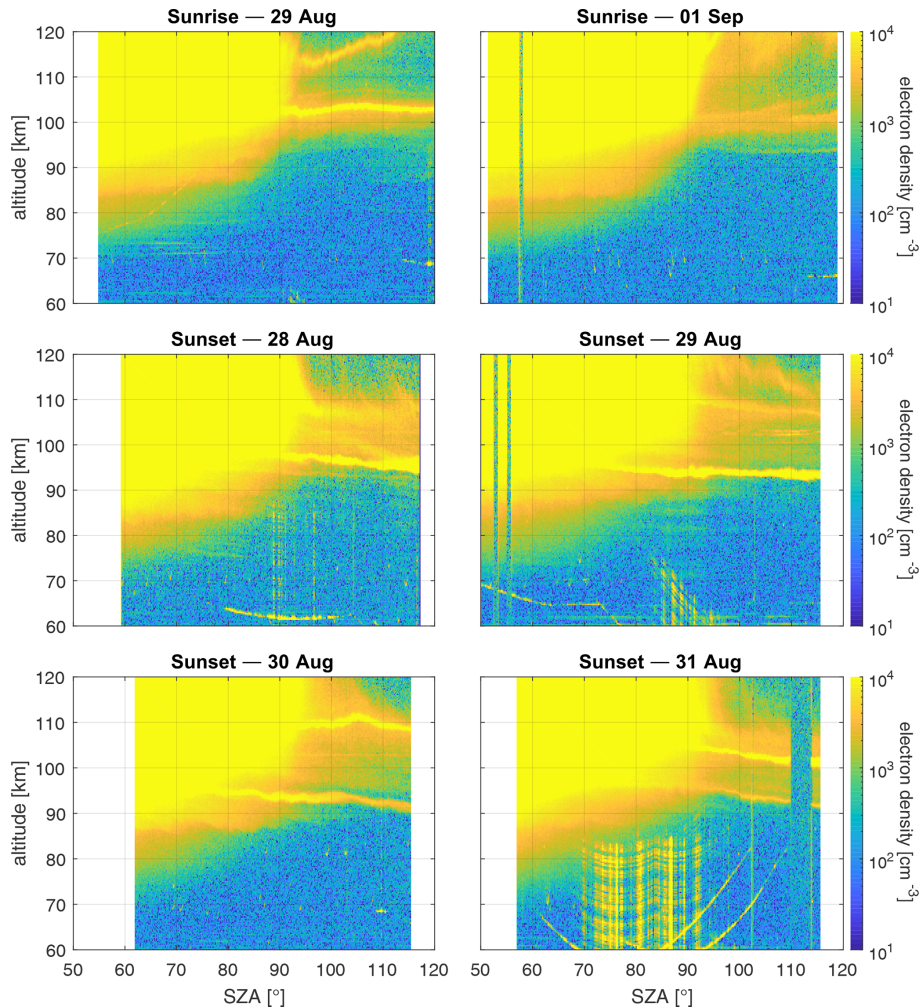


**Figure 1.** Arecibo radar measurements of the electron density from 28 August until 1 September 2016: four successful measurements during sunset and two during sunrise. The  $x$  axis has been set to solar zenith angle (SZA) for better comparability. The maximum value of the colour bar has been intentionally set to  $10^4 \text{ cm}^{-3}$  to highlight low electron density values.

model designed specifically for the D region. It covers the altitude range from 20 to 150 km including an ion chemistry for the most prominent ions. This model has been widely employed across various applications, e.g. for polar energetic particle precipitation (e.g. Verronen et al., 2005) and as the model for inversion of electron density profiles from spectral riometry (Kero et al., 2014).

The SIC model includes a chemical scheme of 41 positive ions, 29 negative ions, and 34 neutral species to represent the D region and the underlying mesosphere and lower thermosphere. The model takes into account ionization processes from solar radiation, precipitating electrons and protons, and galactic cosmic rays. The chemistry scheme includes ion-neutral reactions, electron attachment and detachment, and electron–ion and ion–ion recombination. Vertical transport of some minor neutral species is represented by parameterized eddy and molecular diffusion. But there is no vertical transport of ionized species and no horizontal transport because

SIC is a 1D model. For a more comprehensive description of the SIC model, see Verronen (2006). To represent meteoric smoke particles (MSPs) in SIC, a particle size distribution that is based on Megner et al. (2006) was incorporated into SIC (this version will be called SIC-MSP from now on). To couple the neutral MSP to the D-region ionosphere, SIC-MSP derives the MSP charging rates. SIC-MSP handles direct electron and ion attachment to neutral MSPs as well as charged MSPs. The most relevant MSP-related processes are the electron attachment to neutral MSPs and the consecutive electron photodetachment of negatively charged MSPs induced by sunlight. The interplay of both processes is particularly interesting during sunset and sunrise as during that time the charging and corresponding decharging of the negatively charged MSP fraction occur.

SIC has been extensively used to model the high-latitude ionosphere in combination with EISCAT radar observations. Its application to the low-latitude D region like in Arecibo

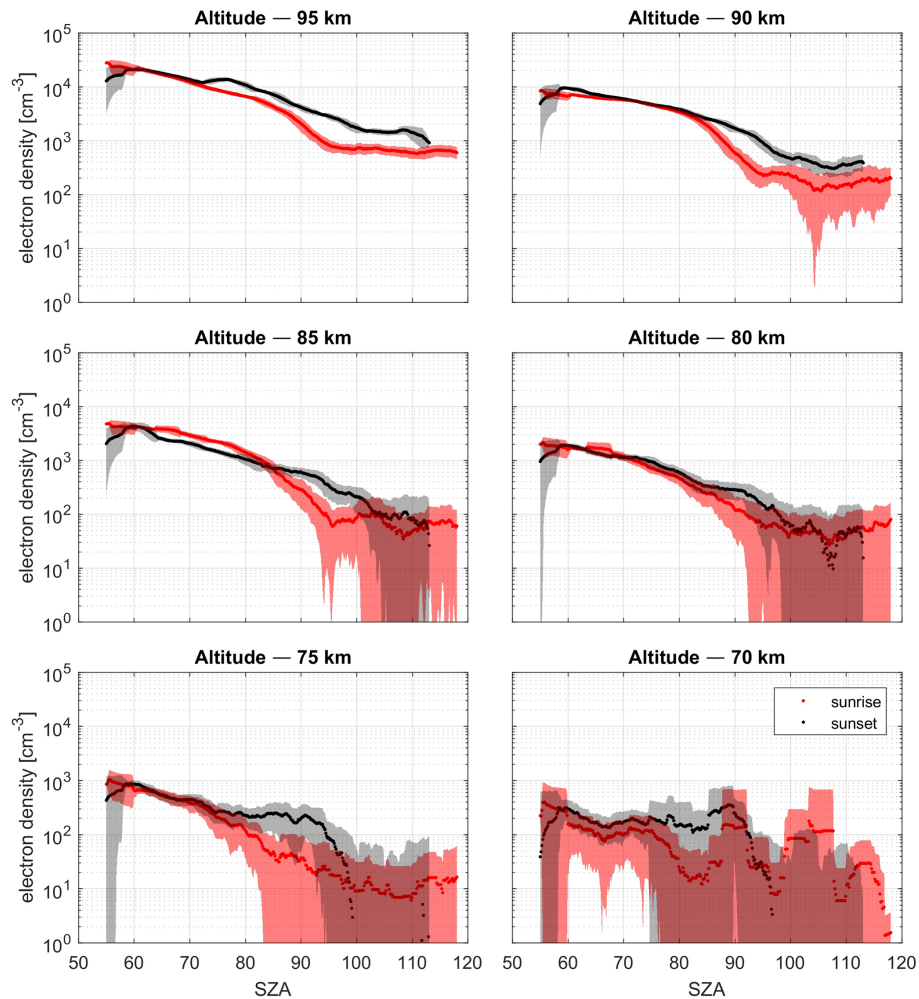


**Figure 2.** Sunset and sunrise comparison of the measured electron density at altitudes of 95 down to 70 km as a function of solar zenith angle (SZA). Solid lines represent the 20-point running mean of two sunrise measurements and four sunset measurements. Shaded areas represent the 20-point running standard deviation. Sunset values represent a 25 % trimmed mean to remove outliers due to sporadic E layers.

(Puerto Rico), however, does not need very specific changes. Photoionization and ionization due to galactic cosmic rays are calculated for the location in question. Of course, particle precipitation as an ionization source is turned off, and besides that only a slight adaptation of the vertical-diffusion coefficient is needed. The individual ion species and involved ion chemistry remain untouched.

The second model being compared to the measurements is the WACCM-D model (Verronen et al., 2016). This global circulation model is a variant of the Whole Atmosphere Community Climate Model (WACCM) that incorporates a D-region ion chemistry scheme based on the SIC model and includes 307 reactions of 20 positive ions and 21 negative ions. For comparison to the electron density measurements performed in 2016 we use model results for the year 2005. By using WACCM-D data from the same season we arrive at similar SZAs, Ly- $\alpha$  fluxes, and overall conditions despite introducing a slight difference due to comparing measure-

ment and model data from different solar cycles. In contrast to SIC, WACCM-D is able to handle the diffusion and transport of all species (neutral and ions), vertically as well as horizontally. However, neither model considers thermospheric plasma transport due to electromagnetic forces or ambipolar diffusion. The WACCM-D model gives out data for the whole globe with a bin size of  $1.9^\circ \times 2.5^\circ$  in latitude and longitude and a 1 h time resolution. For the following analysis we chose latitude  $18^\circ$  N and made use of different longitude bins around the globe. The assumption is that the SZA-driven changes at sunrise and sunset, also on dynamics, are much stronger than any dynamical artefact coming from sampling different longitudes at the same time. Visual inspection of the WACCM-D data shows that no electron density artefacts are present.

The SIC model is run for Arecibo radar's geographical location ( $18.3^\circ$  N,  $66.8^\circ$  W) and for the same time period as the observations. The altitudes covered by WACCM-D and

SIC reach up to 150 km altitude; here we concentrate on the altitude region between 77 and 91 km.

Identical to the Arecibo measurement data, the time axis of the output of both models has been transferred to SZA. The SIC model's time resolution of 5 min transfers into approximately 1° SZA. The 1 h time resolution of the WACCM-D model, however, is much more sparse. To increase the SZA resolution of WACCM-D, output data from all longitudes covered in the spatial resolution are transferred to SZA. By doing so the resolution of the WACCM-D results can be reduced to below 1° SZA. This handling is valid under the assumption that there are only minor longitudinal variations in the D region. This is the case in the low-latitude D-region ionosphere, which is solely governed by photoionization.

In contrast to Fig. 2, the comparison of the electron density measurement with the ionospheric models is separated into sunset and sunrise conditions. Figure 3 shows the mean sunrise measurements as well as the corresponding model results in the left panels. The right panels of Fig. 3 show the sunset comparison of model results and electron density measurements. The altitudes that have been chosen for comparison are 91, 85, 80, and 77 km. These altitudes have been chosen because they closely match the pressure levels of WACCM-D. Measurements at higher altitudes are not compared to the used ionospheric models because these models do not fully cover E-region physics, like sporadic E layers. Measurements at lower altitudes are often too close to or at the noise floor of the radar and are not considered for comparison.

The sunrise comparison in Fig. 3 at 91 km altitude shows a good agreement between SIC/WACCM-D and the measurement at lower SZA. However, the shape of the electron density rise during sunrise is not reproduced with the models. SIC and WACCM-D expect a relative sharp electron density increase, while the measurements indicate a prolonged electron density increase for an extended period. The expected electron density jump of the SIC-MSP model at 100° SZA is not observed.

The sunset comparison in Fig. 3 at 91 km altitude shows good agreement between ionospheric models and the measurements. However, at SZAs < 70° WACCM-D slightly underestimates the electron density. The SIC model overestimates the electron density between 80 and 90° SZA. WACCM-D reproduces the shallow electron decrease during sunset slightly better than the SIC model. The sudden drop of electron density in the SIC-MSP run is within 1 standard deviation of the measurements for SZAs between 100 and 110°.

The measured sunrise electron density at 85 km is very well captured by SIC and WACCM-D as well. The early-morning electron density (high SZA) in WACCM-D is however much lower compared to the SIC model. However, the measurement standard deviation is high at SZA > 90°, which makes a distinction between the models impossible. At SZA greater than 90°, the SIC model is at the upper edge of the

measurements and WACCM-D at the lower edge. Moreover, the SIC-MSP results remain feasible as they repeatedly lie within the standard deviation of the observation.

During sunset at 85 km WACCM-D compares best to the slowly decaying electron density measurements. The SIC model has a slightly steeper electron density drop between 85 and 95° SZA but also shows generally a shallower electron density decay in contrast to the steeper electron rise during the morning hours. The SIC-MSP results are not fully resembled by the standard deviation of the measurement, and a distinct electron density drop is not visible as well.

When going down to lower altitudes like 80 and 77 km, SIC and WACCM-D underestimate the number of free electrons. During the sunrise, WACCM-D still rises from very low electron density. The SIC results show higher nighttime values of electron density; however the increase occurs later at smaller SZAs. The standard SIC as well as the SIC-MSP version show a distinct jump in electron density at around 100° at both altitudes. WACCM-D shows this jump only at the 77 km altitude. These electron density jumps are within the standard deviation of the measurement. However, the mean value does not show this electron jump at 80 km altitude, but at 77 km there is a slight shift to a smaller SZA of 95°.

During sunset the models underestimate the electron density compared to the measurements at altitudes of 80 and 77 km; WACCM-D shows even lower values than SIC. However, both models represent the slow electron density depletion during sunset. WACCM-D produces a slightly smoother decay at 80 km than SIC for SZA < 90°. At higher SZA the electron density in WACCM-D decays faster than in SIC, but both models are within the standard deviation of the electron density measurement. The electron density drop of the SIC-MSP is within the standard deviation again but is not indicated from the mean measured electron density.

### D-region asymmetry

This section investigates the observed D-region asymmetry during sunset and sunrise (60° < SZA < 100°) with the help of SIC and WACCM-D. The investigation concentrates on the ionospheric processes being implemented within these models and how they behave during sunset and sunrise.

The continuity equation of the electron density is central for the description of the ionosphere. It is rather complex in the D region as also negative ions can exist:

$$\frac{d[N_e]}{dt} = \sum_i q_i - \sum_j \alpha_j [e^-][I_j^+] - \sum_k \beta_k [e^-][N_k] + \sum_l \gamma_l [N_l][I_l^-] + \sum_m \gamma_m^p [I_m^-]. \quad (1)$$

Here,  $\sum_i q_i$  is the electron production by ionization, and  $\sum_j \alpha_j [e^-][I_j^+]$  is the electron loss due to electron recombination with positive ions  $i$ . The loss term  $\sum_k \beta_k [e^-][N_k]$

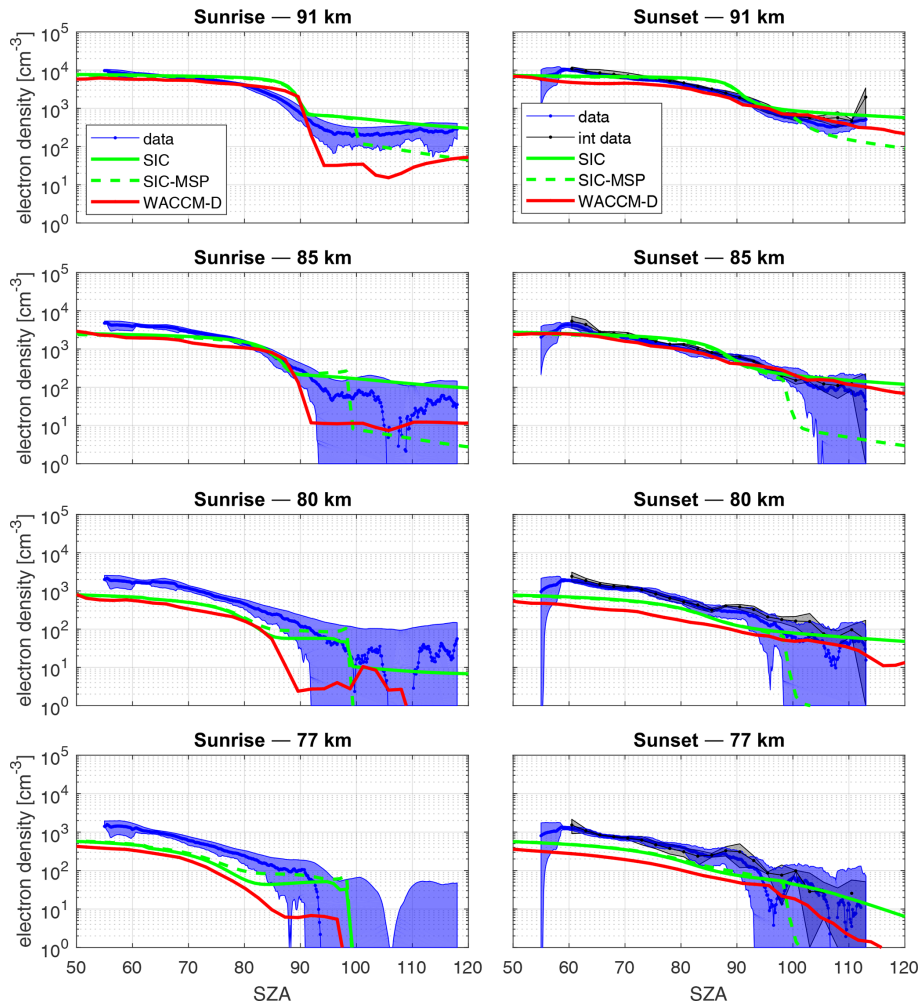


**Figure 3.** Comparison of measured electron densities with model results from the SIC and WACCM-D model for sunrise (left) and sunset (right) at 91, 85, 80, and 77 km altitude. The blue line is the 20-point running mean of the measurements, and the blue area is the corresponding standard deviation. Green lines indicate the SIC model in its standard version (solid) and with meteoric smoke particles incorporated into the ion chemistry (dashed). WACCM-D results are given in red.

describes the electron attachment to neutrals ( $[N_k]$ ), which is important at altitudes below 80 km. Oppositely, the term  $\sum_l \gamma_l [N_l] [I_l^-]$  is the collisional electron detachment from negative ions, while  $\sum_m \gamma_m^p [I_m^-]$  is effective electron detachment by solar photons. The summations and their indices indicate that the ionospheric reactions (Verronen, 2006) are handled with their corresponding reaction partners. The continuity equation above lacks the transport term of the electron density. Direct plasma transport is not considered in SIC and therefore cannot be discussed in this study.

For further analysis Fig. 4 shows all terms of the continuity Eq. (1) during sunrise and sunset for altitudes of 91, 85, and 80 km. The results are based on the SIC model in its standard version without MSP. The given values represent the sum of all individual reaction rates for each term of Eq. (1), i.e. the product of reaction rate coefficient with the appropriate concentrations of the reaction partners.

At 91 km altitude the ionization rate dominates during both sunrise and sunset conditions for SZAs up to  $100^\circ$ . While the electron–ion recombination rate follows closely the ionization rate during sunrise, this is not the case during sunset between  $90$  and  $100^\circ$  SZA. Here, electron–ion recombination rate falls off slower than the ionization rate. At even larger SZA the electron attachment to neutrals and electron detachment from negative ions dominate the continuity equation.

The situation is similar at 85 km. Here as well, ionization rate and electron–ion recombination do not match during sunset. However, the electron attachment to neutrals and detachment from negative ions start to be relevant already. These processes related to negative ions show an asymmetry between sunrise and sunset as well.

At 80 km altitude the situation becomes different. During sunrise the photo-induced electron detachment from the

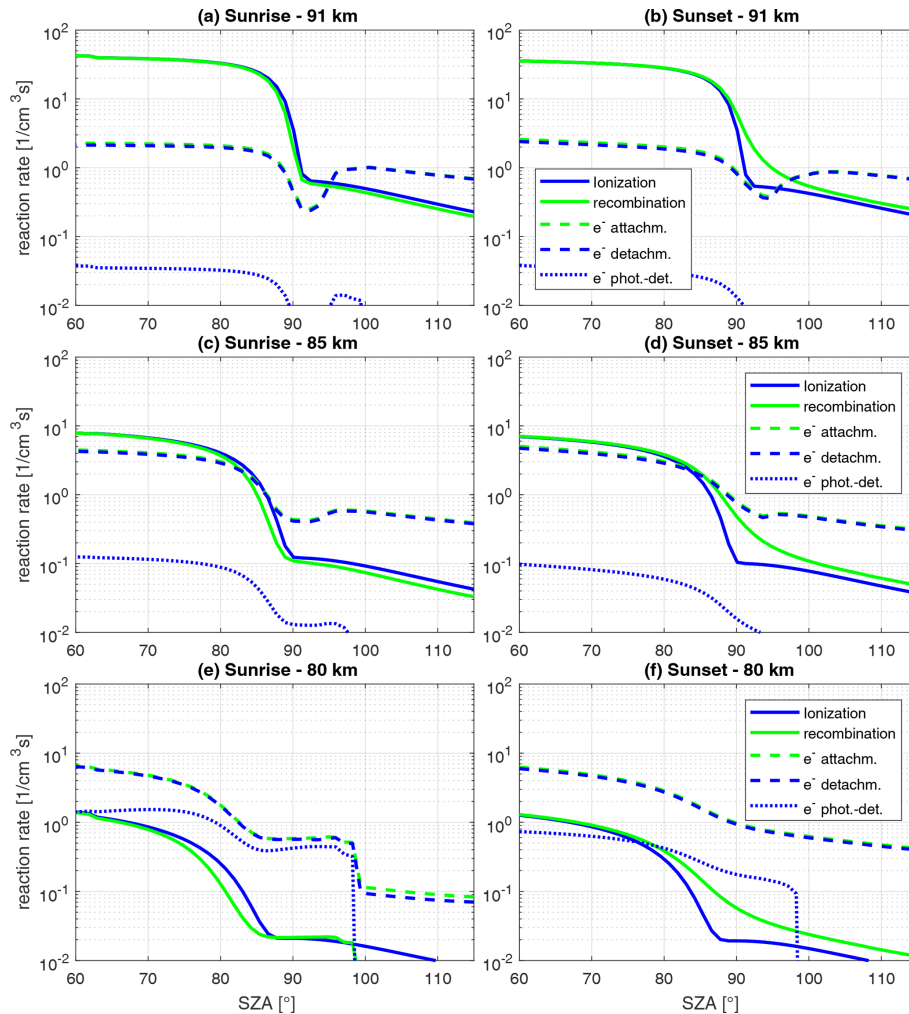


**Figure 4.** Components of the electron continuity Eq. (1) for altitudes 91 km (a, b), 85 km (c, d), and 80 km (e, f) for sunrise (a, c, e) and sunset (b, d, f). The components are the ionization rate (solid blue), electron–ion recombination rate (solid green), electron attachment to neutrals (dashed green), and electron detachment from negative ions (dashed blue). The latter is the sum of collisional detachment (not shown) and photodetachment of electrons from negative ions (dotted blue).

negative-ion reservoir occurs at  $100^\circ$ . This process dominates until this reservoir is emptied; after that the collisional electron detachment is dominant again. The electron–ion recombination rate still falls off slower than the ionization rate during sunset, but the recombination rate also rises slower than the ionization rate during sunrise. But both these processes fall behind the rates of electron attachment to neutrals and electron detachment from negative ions at all times. This results in an asymmetry of the electron density in SIC because both processes show distinct patterns during sunrise and sunset.

#### 4 Discussion

The D-region sunset–sunrise asymmetry is a phenomenon that has been studied for several decades with various tech-

niques. The asymmetry is usually characterized by MF radars measuring the transmitted wave’s Faraday rotation (Coyne and Belrose, 1972) and by oblique radio link amplitudes at different MF frequencies (Laštovička, 1977). We report the first direct measurements of the D-region electron density asymmetry by calibrated incoherent-scatter radar observations.

Here, the D-region electron density during sunrise and sunset is specifically observed by means of ISR radar in Arecibo (Puerto Rico). The observations show significantly lower electron densities during morning hours compared to evening hours when considering SZAs between  $80$  and  $100^\circ$ . For lower SZAs the electron densities do not differ significantly. This asymmetric behaviour is observed for altitudes between  $90$  and  $75$  km altitude.



MF radar observations usually show asymmetries in the observed electron density already starting at SZAs of  $40^\circ$  (Li and Chen, 2014); however they tend to observe at even lower altitudes. The D-region asymmetry has also been observed by means of VLF observations, and these observations also indicate a D-region asymmetry starting at lower SZAs compared to the findings presented in this study. The reason for different observations of the asymmetry remains unclear and is left to be investigated in future studies.

In this study we also conduct a comparison of time-dependent ionospheric models with the measured electron densities. The one-dimensional SIC model and three-dimensional WACCM-D have been used to model the sunset and sunrise electron density. Both models employ equivalent ionospheric reaction schemes. Therefore, SIC and WACCM-D show similar results (cf. Fig. 3), but in the end WACCM-D agrees better with the observations, especially during sunset. The advantage of WACCM-D lies in being a general circulation model. The neutral background of SIC is provided by the NRLMSIS model (Picone et al., 2002), which is a climatological model of the upper atmosphere. The difference between both models has to originate from transport or the background atmosphere's temperature and its representation within either model. For instance, tides can impact the ion chemistry significantly and alter the abundance of heavy water cluster ions (e.g. Forbes, 1982). A thorough analysis of the differences between SIC and WACCM-D, especially in the ionosphere at low latitudes, is subject to a future study.

The performance of both models in comparison to the observations is not so good during sunrise conditions. That can be a result of unknown reaction rate coefficients for electron detachment from some negative ions. Not all negative ions have a direct reaction path to lose electrons but require a detour transfer reaction to a negative-ion species that actually can lose electrons.

The analysis of the electron continuity equation for the SIC model (cf. "D-region asymmetry" section) reveals the underlying processes of the observed D-region asymmetry. At altitudes of 85 and 90 km altitude the interplay between electron–ion recombination rate and ionization rate is most important. During sunset the recombination rate is higher than the ionization rate, but during sunrise both rates match closely. The difference between both rates during sunset can be explained by the fast-declining ionization rate due to Ly- $\alpha$  atmospheric absorption as the sun goes down and the inability of the recombination reactions to follow with the same speed. The remaining electrons and positive ions just need additional time to recombine and reach a steady state with the lower ionization rate later during the night ( $SZA > 100^\circ$ ). At lower altitudes the electron attachment to neutral species and detachment from negative ions are more important and dominate the shape of the asymmetry within SIC. A detailed analysis of these time-dependent processes and an identification of involved ion species, especially for WACCM-D, are the subject of a future study.

The presence of charged meteoric smoke particles (MSPs) has been proven by several rocket-borne and radar observations. These chargeable MSPs are expected to cause distinct jumps and decreases in electron density during sunrise and sunset at D-region altitudes ( $SZA = 100^\circ$ ). A thorough analysis of this experiment, however, does not show these distinct features in the electron density (cf. Sect. 2). However, the comparison of the observation to the SIC-MSP model (Baumann et al., 2015) shows that these features occur during times when the sensitivity of this experiment is not sufficient to test our understanding of MSP effects.

## 5 Conclusions

In this study, we concentrated on the sunset and sunrise behaviour of the D-region ionosphere and measured the electron density with the Arecibo incoherent-scatter radar located in Puerto Rico. A sunset–sunrise asymmetry of the electron density has been observed with the ISR technique for the first time. These observations have been compared to the 1D ionospheric model SIC and the 3D GCM WACCM-D that has the SIC ion chemistry included.

The identified asymmetry in the D-region electron density is a higher electron density during sunset than during sunrise for the same SZAs. This asymmetry was observed for SZAs greater than  $80^\circ$  and in an altitude region between 75 and 95 km. Other studies using MF radar (Coyne and Belrose, 1972; Laštovička, 1977; Li and Chen, 2014, e.g.) and VLF observations (e.g. Thomson et al., 2007; Kumar and Kumar, 2020) reported this D-region asymmetry for lower SZA (down to  $40^\circ$ ) and lower-altitude regions. The present ISR observation showed that the observable time span of the D-region asymmetry decreases with altitude and shifts to higher SZAs.

The observed D-region asymmetry was analysed by comparison to the one-dimensional ionospheric model SIC and the 3D GCM WACCM-D that also includes a similar ion chemistry scheme. Both models, SIC and WACCM-D, show signatures of an asymmetry between sunset decline and sunrise growth of electron density. However, WACCM-D generally reproduces the observed D-region asymmetry better. An analysis of the continuity equation of the ionospheric electron density showed that SIC's asymmetry originated from a higher electron–ion recombination rate than the ionization rate during sunset. As the sun goes down, the electron–ion recombination is not fast enough and needs time to reach a steady state with the rapidly declining ionization rate. At an altitude of 80 km and below, the electron attachment to neutrals and electron detachment from negative ions govern the shape of the D-region electron density during sunrise and sunset here. The differences between SIC and WACCM-D could be attributed to the vertical- and horizontal-transport processes being taken into account in WACCM-D but not in SIC, while the ion chemistry scheme is similar in both mod-

els. It is very likely that the background neutral atmosphere and its temperature and dynamics play a significant role in the D-region ionosphere during times of weak ionization and should be further investigated in the future.

In addition, the D-region observations did not clearly indicate a sudden electron density increase (depletion) caused by discharging (charging) of MSPs during sunrise (sunset) as indicated by specific ionospheric modelling (Baumann et al., 2015) at a SZA of 100°. However, the ISR measurements during these high SZAs lack sensitivity at altitudes below 90 km. The lack of signal power increased the uncertainty in the measured electron density, making an ultimate conclusion impossible or at least ambiguous. Further studies on the optical and charging properties of MSPs and further D-region observations during different times throughout the day remain necessary.

*Code and data availability.* The raw radar data (power profiles and plasma line measurements), processed data, and plotting routines for Figs. 3 and 4 have been made available on Zenodo (<https://doi.org/10.5281/zenodo.6381903>, Baumann et al., 2022).

*Author contributions.* The research idea was conceived by CB, AK, and MR. The radar experiment was conducted by MPS. Data analysis was performed by CB with support from AK, SR, MR, and JV. WACCM-D data were provided by PTV. Interpretation of the results was performed by CB, AK, PTV, and MR. All authors contributed to the writing of the manuscript.

*Competing interests.* The contact author has declared that none of the authors has any competing interests.

*Disclaimer.* Publisher's note: Copernicus Publications remains neutral with regard to jurisdictional claims in published maps and institutional affiliations.

*Acknowledgements.* The authors thank Nestor Aponte and Phil Perillat for their support at the radar site. All authors thank topical editor Dalia Buresova for handling our manuscript during the review process. The authors also thank all three referees for their constructive comments on the initial manuscript.

*Financial support.* The work of Antti Kero is funded by the Tenure Track Project in Radio Science at Sodankylä Geophysical Observatory, University of Oulu. The work of Pekka T. Veronen is supported by the Academy of Finland grant no. 335555 (ICT-SUNVAC). The radar observation itself was funded at the time by National Astronomy and Ionosphere Center (NAIC), National Science Foundation (NSF), and SRI International based on proposal T3087.

The article processing charges for this open-access publication were covered by the German Aerospace Center (DLR).

*Review statement.* This paper was edited by Dalia Buresova and reviewed by three anonymous referees.

## References

- Asmus, H., Robertson, S., Dickson, S., Friedrich, M., and Megner, L.: Charge balance for the mesosphere with meteoric dust particles, *J. Atmos. Sol.-Terr. Phys.*, 127, 137–149, <https://doi.org/10.1016/j.jastp.2014.07.010>, 2015.
- Baumann, C., Rapp, M., Kero, A., and Enell, C.-F.: Meteor smoke influences on the D-region charge balance – review of recent in situ measurements and one-dimensional model results, *Ann. Geophys.*, 31, 2049–2062, <https://doi.org/10.5194/angeo-31-2049-2013>, 2013.
- Baumann, C., Rapp, M., Anttila, M., Kero, A., and Veronen, P. T.: Effects of meteoric smoke particles on the D region ion chemistry, *J. Geophys. Res.-Space*, 120, 10823–10839, <https://doi.org/10.1002/2015JA021927>, 2015.
- Baumann, C., Kero, A., Raizada, S., Rapp, M., Sulzer, M. P., Veronen, P. T., and Vierinen, J.: Arecibo measurements of D-region electron densities during sunset and sunrise in August 2016, Zenodo [data set], <https://doi.org/10.5281/zenodo.6381903>, 2022.
- Breakall, J. K. and Mathews, J. D.: A theoretical and experimental investigation of antenna near-field effects as applied to incoherent backscatter measurements at Arecibo, *J. Atmos. Terr. Phys.*, 44, 449–454, [https://doi.org/10.1016/0021-9169\(82\)90051-4](https://doi.org/10.1016/0021-9169(82)90051-4), 1982.
- Cho, J. Y. N., Sulzer, M. P., and Kelley, M. C.: Meteoric dust effects on D-region incoherent scatter radar spectra, *J. Atmos. Sol.-Terr. Phys.*, 60, 349–357, [https://doi.org/10.1016/S1364-6826\(97\)00111-9](https://doi.org/10.1016/S1364-6826(97)00111-9), 1998.
- Coyne, T. N. R. and Belrose, J. S.: The Diurnal and Seasonal Variation of Electron Densities in the Midlatitude D Region Under Quiet Conditions, *Radio Sci.*, 7, 163–174, <https://doi.org/10.1029/RS007i001p00163>, 1972.
- Evans, J. V.: Theory and practice of ionosphere study by Thomson scatter radar, *Proc. IEEE*, 57, 496–530, <https://doi.org/10.1109/PROC.1969.7005>, 1969.
- Forbes, J. M.: Tidal effects on D and E region ion chemistries, *J. Geophys. Res.*, 86, 1551–1563, <https://doi.org/10.1029/JA086iA03p01551>, 1981.
- Forbes, J. M.: TEMPERATURE AND SOLAR ZENITH ANGLE CONTROL OF D-REGION POSITIVE ION CHEMISTRY, *Planet. Space Sci.*, 30, 1065–1072, [https://doi.org/10.1016/0032-0633\(82\)90157-X](https://doi.org/10.1016/0032-0633(82)90157-X), 1982.
- Friedrich, M. and Rapp, M.: News from the Lower Ionosphere: A Review of Recent Developments, *Surv. Geophys.*, 30, 525–559, <https://doi.org/10.1007/s10712-009-9074-2>, 2009.
- Friedrich, M., Siskind, D. E., and Torkar, K. M.: Haloe nitric oxide measurements in view of ionospheric data, *J. Atmos. Sol.-Terr. Phys.*, 60, 1445–1457, [https://doi.org/10.1016/S1364-6826\(98\)00091-1](https://doi.org/10.1016/S1364-6826(98)00091-1), 1998.
- Friedrich, M., Rapp, M., Blix, T., Hoppe, U.-P., Torkar, K., Robertson, S., Dickson, S., and Lynch, K.: Electron loss and mete-

- oric dust in the mesosphere, *Ann. Geophys.*, 30, 1495–1501, <https://doi.org/10.5194/angeo-30-1495-2012>, 2012.
- Ganguly, S.: The sunrise and sunset transitions in the mesosphere, *J. Atmos. Terr. Phys.*, 47, 643–652, [https://doi.org/10.1016/0021-9169\(85\)90100-X](https://doi.org/10.1016/0021-9169(85)90100-X), 1985.
- Han, F. and Cummer, S. A.: Midlatitude daytime D region ionosphere variations measured from radio atmospheric, *J. Geophys. Res.-Space*, 115, A10314, <https://doi.org/10.1029/2010ja015715>, 2010.
- Hunten, D. M., Turco, R. P., and Toon, O. B.: Smoke and dust particles of meteoric origin in the mesosphere and stratosphere, *J. Atmos. Sci.*, 37, 1342–1357, [https://doi.org/10.1175/1520-0469\(1980\)037<1342:SADPOM>2.0.CO;2](https://doi.org/10.1175/1520-0469(1980)037<1342:SADPOM>2.0.CO;2), 1980.
- Hysell, D. L., Nossa, E., Larsen, M. F., Munro, J., Sulzer, M. P., and González, S. A.: Sporadic E layer observations over Arecibo using coherent and incoherent scatter radar: Assessing dynamic stability in the lower thermosphere, *J. Geophys. Res.-Space*, 114, A12303, <https://doi.org/10.1029/2009JA014403>, 2009.
- Isham, B., Tepley, C. A., Sulzer, M. P., Zhou, Q. H., Kelley, M. C., Friedman, J. S., and Gonzalez, S. A.: Upper atmospheric observations at the Arecibo Observatory: Examples obtained using new capabilities, *J. Geophys. Res.*, 105, 18609–18637, <https://doi.org/10.1029/1999JA900315>, 2000.
- Kero, A., Vierinen, J., Enell, C.-F., Virtanen, I., and Turunen, E.: New incoherent scatter diagnostic methods for the heated D-region ionosphere, *Ann. Geophys.*, 26, 2273–2279, <https://doi.org/10.5194/angeo-26-2273-2008>, 2008.
- Kero, A., Vierinen, J., McKay-Bukowski, D., Enell, C.-F., Sinor, M., Roininen, L., and Ogawa, Y.: Ionospheric electron density profiles inverted from a spectral riometer measurement, *Geophys. Res. Lett.*, 41, 5370–5375, <https://doi.org/10.1002/2014gl060986>, 2014.
- Kudeki, E., Milla, M., Friedrich, M., Lehmacher, G., and Sponseller, D.: ALTAIR incoherent scatter observations of the equatorial daytime ionosphere, *Geophys. Res. Lett.*, 33, L08108, <https://doi.org/10.1029/2005GL025180>, 2006.
- Kumar, A. and Kumar, S.: Ionospheric D-Region Parameters Obtained Using VLF Measurements in the South Pacific Region, *J. Geophys. Res.-Space*, 125, e2019JA027536, <https://doi.org/10.1029/2019ja027536>, 2020.
- Laštovička, J.: Seasonal variation in the asymmetry of diurnal variation of absorption in the lower ionosphere, *J. Atmos. Terr. Phys.*, 39, 891–894, 1977.
- Li, N. and Chen, J.: Asymmetry in diurnal variation of electron density in D region over Kunming, in: 2014 XXXIth URSI General Assembly and Scientific Symposium (URSI GASS), IEEE, 1–4, <https://doi.org/10.1109/URSIGASS.2014.6929739>, 2014.
- Mathews, J. D.: The Effect of Negative Ions on Collision-Dominated Thomson Scattering, *J. Geophys. Res.*, 83, 505–512, <https://doi.org/10.1029/JA083iA02p00505>, 1978.
- Mathews, J. D., Breakall, J. K., and Ganguly, S.: The measurement of diurnal variations of electron concentration in the 60–100 km ionosphere at Arecibo, *J. Atmos. Terr. Phys.*, 44, 441–448, [https://doi.org/10.1016/0021-9169\(82\)90050-2](https://doi.org/10.1016/0021-9169(82)90050-2), 1982.
- Maurya, A. K., Veenadhari, B., Singh, R., Kumar, S., Cohen, M. B., Selvakumaran, R., Gokani, S., Pant, P., Singh, A. K., and Inan, U. S.: Nighttime D region electron density measurements from ELF-VLF tweek radio atmospheric recorded at low latitudes, *J. Geophys. Res.-Space*, 117, A11308, <https://doi.org/10.1029/2012ja017876>, 2012.
- Megner, L., Rapp, M., and Gumbel, J.: Distribution of meteoric smoke – sensitivity to microphysical properties and atmospheric conditions, *Atmos. Chem. Phys.*, 6, 4415–4426, <https://doi.org/10.5194/acp-6-4415-2006>, 2006.
- Nicolet, M. and Aikin, A. C.: The formation of the D Region of the Ionosphere, *J. Geophys. Res.*, 65, 1469–1483, <https://doi.org/10.1029/JZ065i005p01469>, 1960.
- Picone, J. M., Hedin, A. E., Drob, D. P., and Aikin, A. C.: NRLMSISE-00 empirical model of the atmosphere: Statistical comparisons and scientific issues, *J. Geophys. Res.*, 107, 1468, <https://doi.org/10.1029/2002JA009430>, 2002.
- Plane, J. M. C., Saunders, R. W., Hedin, J., Stegman, J., Khamplanov, M., Gumbel, J., Lynch, K. A., Bracikowski, P. J., Gelinias, L. J., Friedrich, M., Blindheim, S., Gausa, M., and Williams, B. P.: A combined rocket-borne and ground-based study of the sodium layer and charged dust in the upper mesosphere, *J. Atmos. Sol.-Terr. Phys.*, 118, Part B, 151–160, <https://doi.org/10.1016/j.jastp.2013.11.008>, 2014.
- Raizada, S., Sulzer, M. P., Tepley, C. A., Gonzalez, S. A., and Nicolls, M. J.: Inferring D region parameters using improved incoherent scatter radar techniques at Arecibo, *J. Geophys. Res.-Space*, 113, 302, <https://doi.org/10.1029/2007JA012882>, 2008.
- Raizada, S., Tepley, C. A., Aponte, N., and Cabassa, E.: Characteristics of neutral calcium and Ca+ near the mesopause, and their relationship with sporadic ion/electron layers at Arecibo, *Geophys. Res. Lett.*, 38, L09103, <https://doi.org/10.1029/2011GL047327>, 2011.
- Rapp, M., Plane, J. M. C., Strelnikov, B., Stober, G., Ernst, S., Hedin, J., Friedrich, M., and Hoppe, U.-P.: In situ observations of meteor smoke particles (MSP) during the Geminids 2010: constraints on MSP size, work function and composition, *Ann. Geophys.*, 30, 1661–1673, <https://doi.org/10.5194/angeo-30-1661-2012>, 2012.
- Reid, I. M.: MF and HF radar techniques for investigating the dynamics and structure of the 50 to 110 km height region: a review, *Progress in Earth and Planetary Science*, 2, 33, <https://doi.org/10.1186/s40645-015-0060-7>, 2015.
- Robertson, S., Dickson, S., Horanyi, M., Sternovsky, Z., Friedrich, M., Janchez, D., Megner, L., and Williams, B.: Detection of Meteoric Smoke Particles in the Mesosphere by a Rocket-borne Mass Spectrometer, *J. Atmos. Sol.-Terr. Phys.*, 118, 161–179, <https://doi.org/10.1016/j.jastp.2013.07.007>, 2013.
- Siskind, D. E., Barth, C. A., and Russell, J. M.: A climatology of nitric oxide in the mesosphere and thermosphere, *Adv. Space Res.*, 21, 1353–1362, [https://doi.org/10.1016/S0273-1177\(97\)00743-6](https://doi.org/10.1016/S0273-1177(97)00743-6), 1998.
- Siskind, D. E., Mlynczak, M. G., Marshall, T., Friedrich, M., and Gumbel, J.: Implications of odd oxygen observations by the TIMED/SABER instrument for lower D region ionospheric modeling, *J. Atmos. Sol.-Terr. Phys.*, 124, 63–70, <https://doi.org/10.1016/j.jastp.2015.01.014>, 2015.
- Strelnikova, I., Rapp, M., Raizada, S., and Sulzer, M.: Meteor smoke particle properties derived from Arecibo incoherent scatter radar observations, *Geophys. Res. Lett.*, 34, L15815, <https://doi.org/10.1029/2007GL030635>, 2007.
- Sulzer, M. P.: A radar technique for high range resolution incoherent scatter autocorrelation function measurements utilizing the

- full average power of klystron radars, *Radio Sci.*, 21, 1033–1040, <https://doi.org/10.1029/RS021i006p01033>, 1986.
- Tanenbaum, S. B.: Continuum Theory of Thomson Scattering, *Phys. Rev.*, 171, 215–221, <https://doi.org/10.1103/PhysRev.171.215>, 1968.
- Thomson, N. R., Clilverd, M. A., and McRae, W. M.: Night-time ionospheric D-region parameters from VLF phase and amplitude, *J. Geophys. Res.-Space*, 112, A07304, <https://doi.org/10.1029/2007ja012271>, 2007.
- Trost, T. F.: Electron concentrations in the E and upper D region at Arecibo, *J. Geophys. Res.-Space*, 84, 2736–2742, <https://doi.org/10.1029/JA084iA06p02736>, 1979.
- Turunen, E., Matveinen, H., Tolvanen, J., and Ranta, H.: D-region ion chemistry model, in: STEP Handbook of Ionospheric Models, edited by: Schunk, R. W., 1–25, SCOSTEP Secretariat, <https://www.bc.edu/content/dam/bc1/offices/ISR/SCOSTEP/Multimedia/other/ionospheric-models.pdf> (last access: 25 July 2022), 1996.
- Verronen, P.: Ionosphere-atmosphere interaction during solar proton events, PhD thesis, University of Helsinki, Faculty of Science, Department of Physical Sciences, <http://urn.fi/URN:ISBN:952-10-3111-5> (last access: 25 July 2022), 2006.
- Verronen, P. T., Seppälä, A., Clilverd, M. A., Rodger, C. J., Kyrölä, E., Enell, C.-F., Ulich, T., and Turunen, E.: Diurnal variation of ozone depletion during the October–November 2003 solar proton events, *J. Geophys. Res.-Space*, 110, A09S32, <https://doi.org/10.1029/2004ja010932>, 2005.
- Verronen, P. T., Andersson, M. E., Marsh, D. R., Kovacs, T., and Plane, J. M. C.: WACCM-D Whole Atmosphere Community Climate Model with D-region ion chemistry, *J. Adv. Model Earth Sy.*, 8, 954–975, <https://doi.org/10.1002/2015MS000592>, 2016.
- Whitehead, J. D.: The formation of the sporadic-E layer in the temperate zones, *J. Atmos. Terr. Phys.*, 20, 49–58, [https://doi.org/10.1016/0021-9169\(61\)90097-6](https://doi.org/10.1016/0021-9169(61)90097-6), 1961.
- Wilcox, R.: The Trimmed Mean, chap. 2.2.3, in: Introduction to Robust Estimation and Hypothesis Testing, Academic Press Elsevier, p. 32, <https://doi.org/10.1016/C2010-0-67044-1>, 2011.
- Yngvesson, K. O. and Perkins, F. W.: Radar Thomson scatter studies of photoelectrons in the ionosphere and Landau damping, *J. Geophys. Res.*, 73, 97–110, <https://doi.org/10.1029/JA073i001p00097>, 1968.